Shear-Induced Gelation of a Liquid Crystalline Polyelectrolyte

Ryan J. Fox[1], Maruti Hegde[1], Amar S. Kumbhar[2], Edward T. Samulski[1], Louis A. Madsen[3], Stephen J. Picken[4], and Theo J. Dingemans[1]*

[1]Department of Applied Physical Sciences and [2]Chapel Hill Analytical and Nanofabrication Laboratory, University of North Carolina at Chapel Hill, 121 South Road, Chapel Hill, NC 27599-3300, USA.

[3]Department of Chemistry and Macromolecules and Interfaces Institute, Virginia Tech, Blacksburg, VA 24060, USA

[4]Faculty of Applied Sciences, Delft University of Technology, Van der Maasweg 9, 2629 HZ Delft, The Netherlands.

Abstract: We report the first example of discontinuous shear-thickening in liquid crystalline solutions of a rigid polyelectrolyte that forms rodlike aggregates. Under steady-shear, the shear stress in low viscosity nematic solutions diverges at large strains due to irreversible shear-induced gelation. From the critical shear rate, we determine a concentration scaling law for the rodlike aggregate length. The shear-induced gels have low moduli with large distances between physical crosslinks and an anomalous concentration scaling. Our observations indicate a shear-induced phase transition drives divergent growth of nematic rodlike aggregates resulting in gelation.

Associating polymers (APs) form transient networks when neighboring chains associate via "stickers" — physical crosslinks formed by intermolecular hydrophobic associations, ionic or dipolar interactions, hydrogen bonding, or metal-ligand coordination.[*1, 2*] Such intermolecular stickers form 'elastically active chains' which dictate the solution viscoelastic properties.[*3*] Shear thickening, i.e. an increase in viscosity with shear rate, is an unusual characteristic of AP solutions. Surfactants that assemble into so-called 'equilibrium polymers', such as worm-like micelles (WLMs), form larger shear-induced structures due to orthokinetic coagulation (i.e. shear-induced growth) resulting in increased viscosity, gelation, and ultimately gel fracture.[*4-13*] Such complex fluids are known to undergo a variety of hydrodynamic and elastic instabilities or shear-induced local concentration fluctuations.[*14-22*] However, these effects have largely been investigated in WLMs,[*4-13*] telechelic polymers,[*23*] or partially hydrolyzed polyacrylamide,[*24*] which are systems with weak intermolecular interactions and flexible backbones.

In this Letter, we report the first example of discontinuous shear-thickening in liquid crystalline solutions of a rigid polyelectrolyte that forms rodlike aggregates in water. The observed behavior is unusual in that the steady-state flow curve is essentially discontinuous at a (concentration-dependent) critical shear rate $\dot{\gamma}_c$. Moreover, an induction period of several million strain units are required to realize shear-induced gelation at $\dot{\gamma}_c$. The magnitude of the shear thickening response systematically increases with increasing polymer concentration. We probed the linear viscoelastic response of the shear-induced gels using both time-temperature (TTS) and time-concentration (TCS) superposition principles, enabling construction of a master curve spanning over 20 decades in frequency and 5 decades in dynamic moduli. The shear-induced gel network remains solid-like on experimental time scales as low as 10^{-17} rad s^{-1}, in contrast to other transient physical networks which become liquid-like at much higher frequencies. Analysis of the shear-induced gel structure using scanning electron microscopy (SEM) reveals a porous open-cell structure, consistent with a macroscopic phase separation event. Taken together, these data indicate that a shear-induced phase transition drives divergent growth of rodlike aggregate length resulting in phase separation and gelation.

The polyelectrolyte we used for this study is the sulfonated all-aromatic polyamide, 2,2'-disulfonyl-4,4'-benzidine terephthalamide (PBDT), shown in **Fig. 1**.[*25-32*] PBDT is a water-soluble polyanion with a molecular diameter of ~0.4 nm.[*29*] The PBDT chains self-assemble into dimers (diameter ≈ 0.8 nm), reported to form a double helix based on X-ray, NMR and molecular dynamics simulations.[*28, 31*] The dimers undergo linear aggregation to form high aspect ratio, rodlike aggregates with a mean length $\langle L_0 \rangle$ which we expect to depend on concentration, ionic strength, shear rate $\dot{\gamma}$, and molecular weight.[*8, 31, 33, 34*] PBDT rodlike aggregates should be considered as a type of equilibrium polymer, analogous to WLMs, since the aggregation number N_p and thus $\langle L_0 \rangle$ are thermodynamic quantities and not determined by the synthetic procedure per se.[*35*] These extremely rigid and high aspect ratio rodlike aggregates, with lengths on the order of 10^2–10^3 nm, form a nematic liquid crystalline phase above a relatively low critical concentration (~1 wt.%). Herein, we focus on the effect of concentration and $\dot{\gamma}$ on the structure and rheological properties of these nematic solutions.

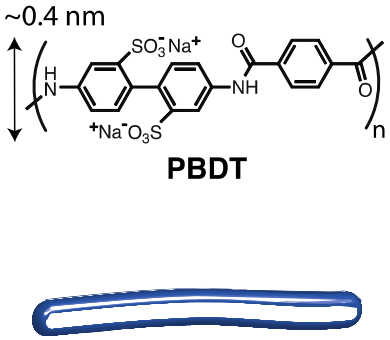

Fig. 1. Molecular structure and self-assembly of PBDT chains into high aspect ratio rodlike aggregates. The dimensions are not drawn to scale.

We performed steady-shear experiments with a strain-controlled ARES G2 rheometer using a cylindrical Taylor-Couette geometry having an outer rotating cylinder and fixed inner cylinder with a recessed end (height H = 41.518 mm, inner radius R_i = 13.829 mm, gap e = 1.171 mm). A minimum of 10 mL was used for each experiment, which fully covered the entire cylinder and mitigated any surface

effects. The temperature was controlled with a Peltier thermoelectric device and fixed at T = 25 °C for all measurements while a solvent trap prevented evaporation of water. The samples of interest range in concentration from 10–30 wt.% polymer with pH = 9, a regime where the solutions exceed the overlap (c^* = 0.16 wt.%) and entanglement (c_e = 1.2 wt.%) concentrations, evidenced by the steady-state viscosity η shown in **Fig. 2A**, i.e. they are semi-dilute entangled solutions.[*36-38*] Power law scaling regimes for the dilute, semi-dilute unentangled, and semi-dilute entangled regime in the isotropic state are given in **Fig. S1**. The local maximum in the η-concentration function at c_1 = 1.9 wt.% corresponds to the isotropic-nematic (I-N) transition.[*39*] The decrease in η above c_1 is due to formation of a locally aligned nematic phase which can be oriented along the flow direction. Standing solutions phase separate into isotropic and nematic phases at a concentration of 2 wt.%, in close agreement with the value from steady-shear experiments. We use this critical concentration (2 wt.%) to estimate the length of rodlike aggregates using the Onsager theory for the I-N transition of anisotropic particles $\phi^* \cong 4d/L$.[*40, 41*] Taking $\phi^* \approx 0.015$ using the bulk PBDT density of 1.35 g cm^{-3}, and the diameter (~0.8 nm) of PBDT rodlike aggregates,[*28, 31*] we estimate the length to be ~215 nm in the quiescent state. Here, we assume that the persistence length l_p is greater than the aggregate contour length, i.e. the rigid-rod regime. This value should be considered an approximate upper bound, as the rodlike aggregates with the longest length will preferentially partition into the nematic phase.[*42*]

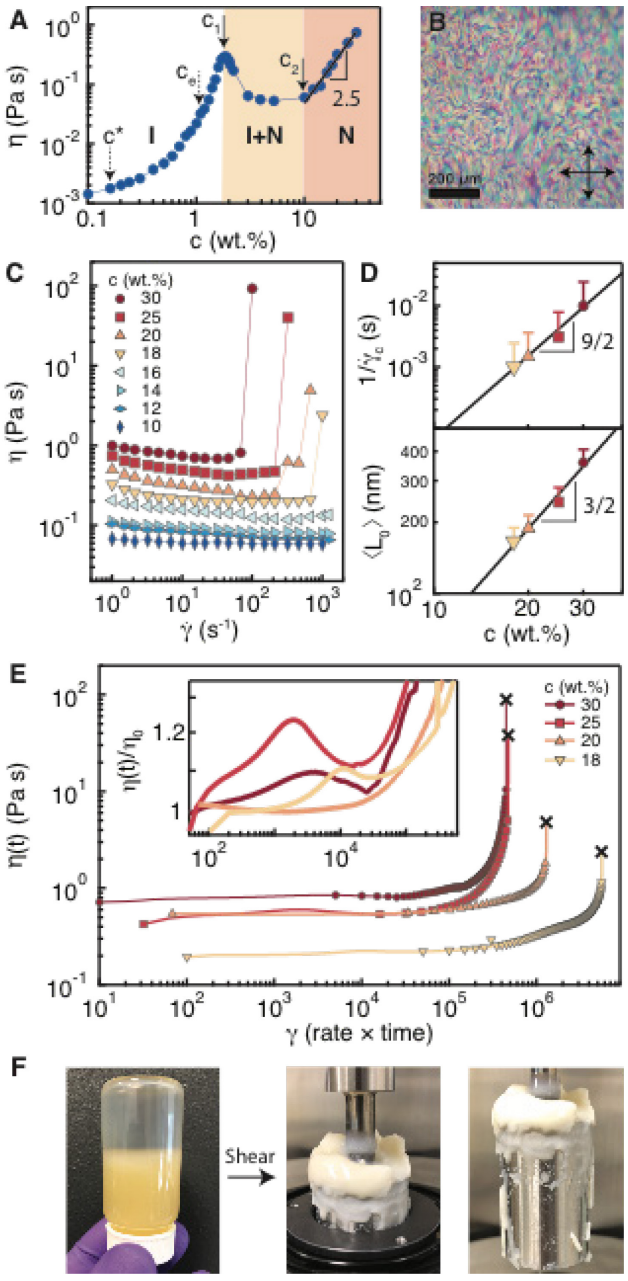

Fig. 2. Steady-state and transient non-linear shear rheology of nematic PBDT solutions. **(A)** Steady-state viscosity as a function of concentration from the dilute, unentangled, isotropic regime to the semi-dilute, entangled, nematic regime (I = Isotropic, I+N = Biphasic, N = Nematic). **(B)** Polarized optical micrograph of a polydomain nematic PBDT solution at 10× magnification. **(C)** Steady-state viscosity flow curves for 10–30 wt.% PBDT nematic solutions. The last data point for samples that shear thicken is taken as the maximum recorded viscosity value during shear-induced gelation before sample expulsion from the rheometer. **(D)** The inverse critical shear rate (top) corresponding to the onset of discontinuous shear thickening and average length (bottom) of the rodlike aggregate, calculated by **Eqn. 1**, as a function of

concentration. **(E)** Transient viscosity at the critical shear rate as a function of dimensionless strain (shear rate × time). The black crosses mark the termination of the experiment due to sample expulsion from the shearing gap. The inset shows the normalized transient viscosity during the induction period, magnified for clarity. **(F)** Digital photographs demonstrate the transition of a 25 wt.% PBDT sample from a low viscosity nematic solution prior to shear (left) to a physical gel (right) after being expelled from rheometer due to shear-induced gelation.

The biphasic region, i.e. coexistence of I-N phases, spans a wide concentration region between 1.9 and 10 wt.% in part because of the high dispersity of rodlike aggregate lengths.[*43*] The detailed mesoscopic structure and liquid crystal phase diagram for PBDT is a sensitive function of molecular weight, salt concentration, and pH and will be the subject of a future publication.[*26, 27, 31, 32*] In this work, stable nematic PBDT solutions that do not phase separate are obtained above c_2 = 10 wt.%. The plateau viscosity η is taken as an average value between $\dot{\gamma}$ = 1–10 s^{-1} and increases above c_2 as $\eta \sim c^{2.5}$ up to 30 wt.%. Under polarized optical microscopy above c_2, the quiescent solutions exhibit a characteristic Schlieren texture consistent with homogeneous nematic phase behavior (**Fig. 2B**) with a local order parameter of ~0.8 at 25 °C from SAXS and ^{2}H NMR measurements.[*28*] However, in the quiescent state, the solutions are globally isotropic due to the random orientations of the locally aligned nematic domains.

Fig. 2C shows the steady-state viscosity flow curves for nematic PBDT solutions between 10–30 wt.% ($c > c_2$). The steady-state viscosities are determined by monitoring the shear stress σ over time at a fixed $\dot{\gamma}$ until a constant stress is attained. Flow curves between 10 and 14 wt.% appear nearly Newtonian over the investigated $\dot{\gamma}$ range. However, the transient response of these solutions exhibits complex stress oscillations characteristic of nematic LCPs.[*44*] We note a slight upturn in η between $\dot{\gamma}$ = 1–10 s^{-1} with increasing concentrations, likely due to Region I shear thinning. Region I shear thinning is associated with increasing contribution of Frank elasticity due to the nematic polydomain texture, and contributes to the increase in η above c_2.[*44, 45*]

The 16 wt.% solution marks the minimum concentration required for the onset of steady-state shear thickening. At $\dot{\gamma}$ = 100 s^{-1}, a small decrease in viscosity is observed, coinciding with extremely long lived transient σ overshoots that require large strains to subside. Extensive analysis of these σ transients is not undertaken here and will be the subject of a future investigation. At $\dot{\gamma}$ > 460 s^{-1}, the steady-state η begins to smoothly increase. The η increases up to $\dot{\gamma}$ = 1230 s^{-1}, but no discontinuities in the flow curve occur at this concentration over the accessible $\dot{\gamma}$ range. At $\dot{\gamma}$ = 680 s^{-1}, we observed sustained σ oscillations for over 10^6 strain units under steady-shear, i.e. rheochaos (see **Fig. S2A**). Slightly higher shear rates ($\dot{\gamma}$ = 1000 s^{-1}) result in a steady-state σ within 150 × 10^3 strain units (see **Fig. S2B)**. These qualitative observations strongly indicate complex spatiotemporal dynamics occurring within the flow due to a non-equilibrium shear-induced structure.

At 18 wt.%, the flow curve is qualitatively similar to the 16 wt.% flow curve with similar stress transients at low $\dot{\gamma}$. However, the order of magnitude discontinuity in the 18 wt.% steady-state η at $\dot{\gamma}$ = 1000 s^{-1} represents a stark departure from the behavior observed at lower concentrations. Higher concentrations (20–30 wt.%) produce larger discontinuities in η which occur at lower $\dot{\gamma}$. In fact, the final viscosity values shown are an underestimate, as gelation causes significant increases in normal stresses that results in sample expulsion from the shearing gap, which in turn terminates the experiment.

The inverse critical shear rate, or relaxation time ($\tau \approx 1/\dot{\gamma}_c$), for onset of divergent shear thickening as a function of concentration is given in **Fig. 2D** (top). The onset of discontinuous shear thickening shifts systematically to lower $\dot{\gamma}$ with increasing concentration. The $\dot{\gamma}_c$ are in agreement with values for rigid rodlike particles under simple shear flow as predicted by Bruinsma et al.[*8*] The relaxation times are on the order of 10^{-3}–10^{-2} s and scale with concentration as $1/\dot{\gamma}_c \sim c^{9/2}$. We use these data to estimate the concentration dependence of $\langle L_0 \rangle$ for PBDT rodlike aggregates below. It has been found that the onset of discontinuous growth of rodlike aggregates in shear flow occurs when the Peclet number $Pe = \dot{\gamma}/D_r$, where D_r is the rotational diffusion constant, is of order unity.[*8, 11*] From this definition, the critical shear rate for shear-induced growth and gelation of rodlike particles of mean length $\langle L_0 \rangle$ is given as[*8*]

$$\dot{\gamma}_c = \frac{k_B T}{\eta_s \langle L_0 \rangle^3} \quad (1)$$

where $k_B T$ is the thermal energy and η_s is the solvent viscosity. We emphasize that this $\langle L_0 \rangle$ is the mean length under *zero shear* and undergoes significant temporal evolution at $\dot{\gamma} \geq \dot{\gamma}_c$. Using this relationship and the measured values of $\dot{\gamma}_c$, we plot $\langle L_0 \rangle$ as a function of concentration in **Fig. 2D** (bottom). The calculated values are in agreement with the aggregate length calculated by the I-N transition concentration. Notably, this is the first determination of the concentration dependence of $\langle L_0 \rangle$ for PBDT rodlike aggregates in solution. The concentration scaling $\langle L_0 \rangle \sim c^{3/2}$ is three times stronger than the classic result for WLMs, which scales as $c^{1/2}$.[*46*] The stronger concentration dependence of $\langle L_0 \rangle$ is likely due to the strong Coulombic interactions for salt-free PBDT solutions; these interactions favor the formation of end-caps, and thus shorter aggregates, as theoretically derived for low ionic strength and highly charged WLMs.[*33*] The electrostatic interactions at low ionic strength results in an apparent power law in the semi-dilute regime $\langle L_0 \rangle \sim c^{1/2\,(1+\Lambda)}$with $\Lambda > 0$, indicating $\Lambda \approx 2$ in our system.[*33*] However, the effect of the nematic orientational ordering on the growth law for $\langle L_0 \rangle$ is not known. Nonetheless, as our solutions are in the entangled, semi-dilute regime and the dimensionless concentration is $\bar{C} = \phi_L \langle L \rangle^3 \gg 1$, divergent growth of rodlike aggregates is expected to strongly proceed via spinodal decomposition resulting in shear-induced gelation.[*8*]

The transient viscosities $\eta(t)$ at $\dot{\gamma} = \dot{\gamma}_c$ for samples between 18–30 wt.% are shown as a function of dimensionless strain (γ = rate × time) in **Fig. 2E**. Overall, we observe strong rheopectic behavior, where $\eta(t)$ increases with time at constant $\dot{\gamma}$. After an induction period between 10^5–10^7 strain units, $\eta(t)$ increases by orders of magnitudes over the initial value, with rapid acceleration at the highest strains. During the induction period, $\eta(t)$ goes through a local maximum possibly related to the formation and breakdown of a meta-stable network structure, see the inset of **Fig. 2E**. The total γ required for shear-induced gelation tends to decrease with increasing concentration, with induction times on the order of 10^3–10^4 s. We do not further explore the kinetics of the shear-induced gelation and focus the rest of this Letter on the structure and properties of the final gels. The transition from a low viscosity fluid to a

physical gel is demonstrated by the digital photographs in **Fig. 2F** before loading (left) and after the experiment is terminated (right), evidencing a dramatic change in both physical and optical properties. The change in the color of the solutions, from yellow to white after shearing, suggests the formation of mesoscopic shear-induced structures that strongly scatter visible light.[*6*] The two most striking features of these data are the ultra-long induction time prior to gelation and the magnitude in the change of η during irreversible shear-induced gelation.

We investigated the viscoelastic behavior of the shear-induced PBDT gels prepared from the experiments shown in **Fig. 2** with linear shear rheology. We used a parallel plate geometry with diameters D = 50 mm or 25 mm and coated the edges with a low viscosity oil to prevent water evaporation. Isothermal frequency sweeps from 100 to 0.1 rad s^{-1} were measured in 5 °C intervals between 25 and 75 °C. Strain amplitudes less than 1% were used to probe the response in the linear viscoelastic regime. We utilized TTS to horizontally shift each isotherm along the frequency axis to construct master curves at T_{ref} = 25 °C spanning nearly 10 decades in frequency for each concentration (**Fig. S3A**). These data conclusively show the substantial increase in network connectivity after shear-induced gelation and with increasing concentration. Furthermore, we collapsed the concentration series using TCS to generate a single master curve spanning over 20 decades in frequency and over 5 decades in dynamic moduli at c_{ref} = 30 wt.%, given in **Fig. 3A**.

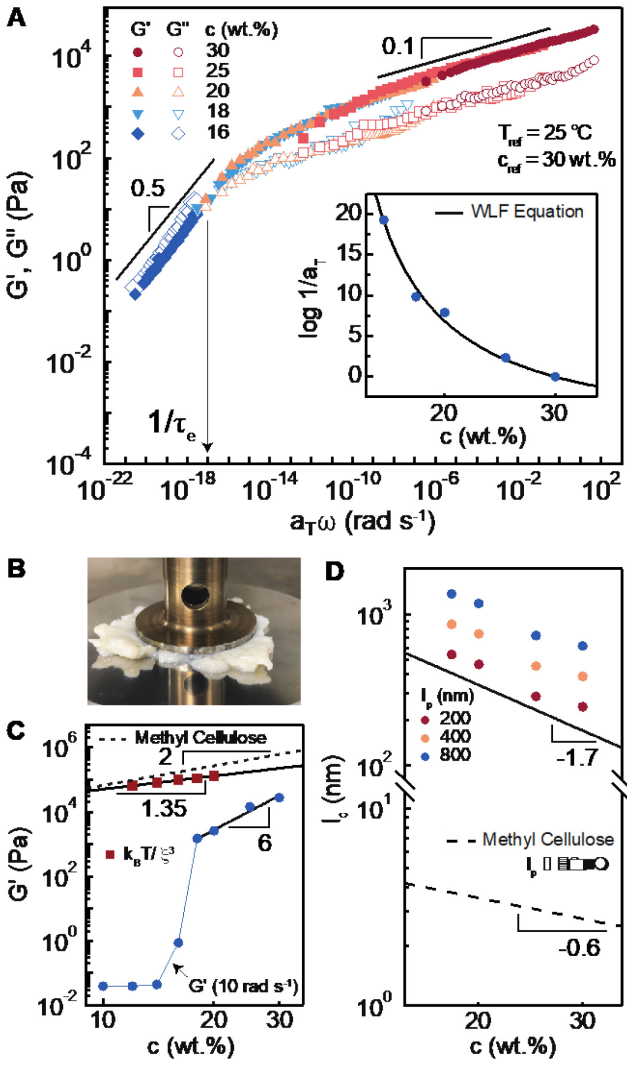

Fig. 3. Linear oscillatory rheology of shear-induced PBDT gels. **(A)** Storage (G', filled symbols) and loss (G", open symbols) moduli master curve as a function of shifted frequency from time-temperature superposition (TTS) at T_{ref} = 25 °C and time-concentration superposition (TCS) at c_{ref} = 30 wt.%. The entanglement lifetime ($1/\tau_e$) is found at the crossover of G' and $G"$. **(Inset)** Shift factors derived from TCS as function of concentration. The solid line is a fit using the William-Landel-Ferry (WLF) equation given by **Eqn. 2**. **(B)** Digital photograph of the shear-induced gel after loading into the parallel plate rheometer prior to trimming the edges, evidencing solid-like behavior. **(C)** G' at 10 rad s^{-1} and 25 °C (filled circles) for shear-induced gels as a function of concentration. The calculated G' based on polyelectrolyte scaling theory ($G' \approx k_BT/\xi^3$) for an isotropic network is shown (filled squares). The extrapolated G' for an isotropic methyl cellulose (MC) gel is given for comparison (dashed line) from ref [*47*]. **(D)** Calculated distance between crosslinks (l_c) calculated from **Eqn. 3** as a function of concentration

for the shear-induced gels. The extrapolated l_c for MC gels is given for comparison. Power law scaling exponents are given in the figures.

The collapse of the data using TTS and TCS indicates that the nature of the gel structure is concentration independent. The shift factors used in TCS a_T are plotted in the inset of **Fig. 3** and appear to be well described by a modified William-Landel-Ferry (WLF) equation given as

$$\log 1/a_T = \frac{\mathrm{A}(c-c_{ref})}{\mathrm{B}+(c-c_{ref})} \qquad (2)$$

where $\mathrm{A} = -5.5 \pm 1.0$ and $\mathrm{B} = 18.0 \pm 0.8$ are empirical constants obtained from fitting and c_{ref} = 30 wt.%. The applicability of the WLF equation to the data confirms we are measuring a true viscoelastic phase transition over the investigated frequency range. The fibrous shear-induced gel, seen in **Fig. 3B**, exhibits a solid-like viscoelastic response ($G' > G"$) with a nearly frequency independent modulus ($G' \sim \omega^{0.1}$) observed over a wide range of frequencies down to the entanglement lifetime of $1/\tau_e \approx 10^{-17}$ rad s^{-1}. At frequencies below $1/\tau_e$, Rouse-like dynamics (G', $G" \sim \omega^{1/2}$) are observed over the 5 lowest decades in frequency and no terminal flow behavior ($G' \sim \omega^2$, $G" \sim \omega^1$) occurs over the experimentally accessible frequency range. A Cole-Cole plot, where G" is plotted vs G', lacks the signature semi-circle shape of an ideal Maxwell fluid as found for WLMs[*46*], confirming that the gels have a broad spectrum of relaxation times (see **Fig. S3B**).[*35*] These data indicate that "sticky interactions", i.e. physical crosslinking sites between rodlike aggregates, dominate the viscoelastic dynamics and are largely temperature insensitive.[*3*]

The scaling of G' with concentration, given in **Fig. 3C**, highlights the unusual structure of the shear-induced gels. The inflection in G' by more than 3 decades (1 Pa to >kPa) between 16 to 18 wt.% corresponds to the onset of shear-induced gelation (see **Fig. 2C**). As a means of comparison, we calculate G' using polyelectrolyte scaling theory[*3, 37*] $G' \approx k_B T/\xi^3$, where ξ is the correlation length determined from the SAXS structure factor peak (see **Fig. S4**), and the experimentally measured G' for a methyl cellulose (MC) model fibrillar gel.[*47*] The shear-induced gels exhibit a remarkably low ($G' \approx$ 1–30 kPa)

which is clearly evidenced when compared to the scaling theory calculation and model MC gel. Above 18 wt.%, the concentration scaling of G' is dramatically higher ($G' \sim c^6$) than both the scaling calculations ($G' \sim c^{1.35}$) and typical fibrillar gels ($G' \sim c^{2-2.5}$).[*47-50*] To gain insight into the gel network structure, we calculate the distance between physical crosslinks l_c using a model for the shear modulus G_0 of fibrillar gels[*51*]

$$G_0 = 6\rho k_B T \frac{l_p^2}{l_c^3} \qquad (3)$$

where $\rho = \phi/\pi r^2$ is the filament-length density, ϕ is the polymer volume fraction, r is the fibril radius, and l_p is the persistence length. The value of l_p for PBDT rodlike aggregates is not precisely known; it is at least 200 nm based on the I-N transition concentration reported here, but could be up to 1 μm or higher.[*31*] **Fig. 3D** shows the calculated values of l_c using various values of l_p (200, 400, and 800 nm) as a function of concentration, which scales as $l_c \sim c^{-1.7}$. The $l_c \approx$ 100–1000 nm for PBDT shear-induced gels are much higher than the model MC gel, where $l_c \approx$ 1–10 nm for similar concentrations and scales as $l_c \sim c^{-0.6}$.[*47, 49*] Instead, shear-induced PBDT gels have very large l_c resulting in a low modulus gel network. We speculate that this discrepancy originates from the locally aligned (nematic) rodlike aggregates that grow during shear-induced gelation, which inhibit physical crosslinking nodes. Thus, shear-induced gelation of nematic fibrillar solutions represents a novel route to fabricate soft gels with high volume fraction polymer, inaccessible to isotropically oriented fibrillar networks.

To qualitatively investigate the PBDT shear-induced gel network structure, we freeze-fractured the pre-shear solutions and shear-induced gels for imaging with SEM. The cross-section of a 16 wt.% PBDT gel pre-shear (**A, B**) and post-shear (**C, D**) is shown in **Fig. 4**. We observe an increase in polymer heterogeneity after shear-induced gelation and development of an open-cell structure with pores on the order of 10 μm. The local alignment of fibrillar structure appears more disordered at length scales on the order of 1 μm, consistent with an elastic instability during gelation causing . The heterogeneous porous structure is consistent with a shear-induced spinodal decomposition process, which is responsible for the observed gelation.[*8*] Indeed, in-situ light sheet microscopy[*6*] and other freeze-fracture[*13*] studies of

shear-thickening WLMs have shown heterogeneous domains on the order of microns or larger. However, our measurement is not an in-situ observation and interpretation of such images should be taken with due caution.

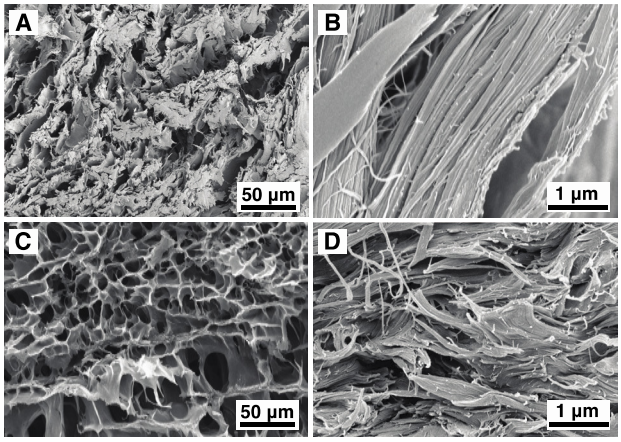

Fig. 4. Scanning electron microscopy (SEM) images of the cross-section surface of a freeze-fractured 16 wt.% PBDT sample **(A, B)** pre- and **(C, D)** post-shear. An open-cell structure consistent with macrophase separation is observed in the post-shear gels. The local fibrillar structure appears more disordered in the post-shear gels.

To conclude, we have reported the first example of a liquid crystalline polyelectrolyte which undergoes discontinuous shear thickening. We observed complex stress transients and a dramatic change in physical properties during irreversible shear-induced gelation. We suggest that a shear-induced phase transition results in the divergent growth of nematic PBDT aggregates causing gelation. Using the onset of discontinuous shear thickening, we determined growth laws for the length of charged PBDT rodlike aggregates as a function of concentration $\langle L_0 \rangle \sim c^{3/2}$, which is consistent with prior theory incorporating electrostatics. The shear-induced gels have low storage moduli ($G' \approx$ 1–30 kPa) and an unusual concentration dependence $G' \sim c^6$ due to the large values of l_c. We propose that the nematic ordering of fibrillar structures inhibits crosslinking nodes and reduces the moduli relative to isotropic networks. More generally, this work provides insights into the complex flow behavior of rodlike aggregates of liquid crystal polyelectrolytes as a new class of shear-thickening fluids.

We thank Ehssan Nazokdast for fruitful discussions and Maggie Daly for assistance with freeze drying of samples for SEM analysis. This material is based upon work supported by, or in part by, the U.S. Army Research Laboratory and the U.S. Army Research Office under contract number A17-0053-001. This work was performed in part at the Chapel Hill Analytical and Nanofabrication Laboratory (CHANL), and Duke University Shared Materials Instrumentation Facility (SMIF), members of the North Carolina Research Triangle Nanotechnology Network (RTNN) which is supported by the National Science Foundation, Grant ECCS-1542015, as part of the National Nanotechnology Coordinated Infrastructure (NNCI). This work benefited from the use of the SasView application, originally developed under NSF Award DMR-0520547. SasView also contains code developed with funding from the EU Horizon 2020 programme under the SINE2020 project Grant No 654000.

See Supplemental Material at [***URL will be inserted by publisher***] for additional rheological and SAXS data.

***Corresponding Author**

E-mail: tjd@unc.edu

References

1. L. Leibler, M. Rubinstein, R. H. Colby, Dynamics of reversible networks. *Macromolecules* **24**, 4701-4707 (1991).
2. M. J. Ballard, R. Buscall, F. A. Waite, The theory of shear-thickening polymer solutions. *Polymer* **29**, 1287-1293 (1987).
3. M. Rubinstein, A. N. Semenov, Dynamics of Entangled Solutions of Associating Polymers. *Macromolecules* **34**, 1058-1068 (2001).
4. Y. T. Hu, P. Boltenhagen, D. J. Pine, Shear thickening in low-concentration solutions of wormlike micelles. I. Direct visualization of transient behavior and phase transitions. *Journal of Rheology* **42**, 1185-1208 (1998).
5. Y. T. Hu, P. Boltenhagen, E. Matthys, D. J. Pine, Shear thickening in low-concentration solutions of wormlike micelles. II. Slip, fracture, and stability of the shear-induced phase. *Journal of Rheology* **42**, 1209-1226 (1998).

6. C.-H. Liu, D. J. Pine, Shear-Induced Gelation and Fracture in Micellar Solutions. *Phys. Rev. Lett.* **77**, 2121-2124 (1996).
7. Y. Hu, S. Q. Wang, A. M. Jamieson, Rheological and flow birefringence studies of a shear-thickening complex fluid—A surfactant model system. *Journal of Rheology* **37**, 531-546 (1993).
8. R. Bruinsma, W. M. Gelbart, A. Ben-Shaul, Flow-induced gelation of living (micellar) polymers. *The Journal of Chemical Physics* **96**, 7710-7727 (1992).
9. S. Hofmann, A. Rauscher, H. Hoffmann, Shear Induced Micellar Structures. *Ber. Bunsenges. Phys. Chem.* **95**, 153-164 (1991).
10. I. Wunderlich, H. Hoffmann, H. Rehage, Flow birefringence and rheological measurements on shear induced micellar structures. *Rheol Acta* **26**, 532-542 (1987).
11. M. E. Cates, M. S. Turner, Flow-Induced Gelation of Rodlike Micelles. *Europhys. Lett.* **11**, 681-686 (1990).
12. P. Boltenhagen, Y. Hu, E. F. Matthys, D. J. Pine, Observation of Bulk Phase Separation and Coexistence in a Sheared Micellar Solution. *Phys. Rev. Lett.* **79**, 2359-2362 (1997).
13. S. L. Keller, P. Boltenhagen, D. J. Pine, J. A. Zasadzinksi, Direct Observation of Shear-Induced Structures in Wormlike Micellar Solutions by Freeze-Fracture Electron Microscopy. *Phys. Rev. Lett.* **80**, 2725-2728 (1998).
14. J. B. Salmon, A. Colin, S. Manneville, F. Molino, Velocity profiles in shear-banding wormlike micelles. *Phys. Rev. Lett.* **90**, 228303 (2003).
15. J. Sprakel, E. Spruijt, M. A. Cohen Stuart, N. A. M. Besseling, M. P. Lettinga, J. van der Gucht, Shear banding and rheochaos in associative polymer networks. *Soft Matter* **4**, (2008).
16. J. Billen, M. Wilson, A. R. C. Baljon, Shear banding in simulated telechelic polymers. *Chemical Physics* **446**, 7-12 (2015).
17. P. E. Boukany, S. Q. Wang, S. Ravindranath, L. J. Lee, Shear banding in entangled polymers in the micron scale gap: a confocal-rheoscopic study. *Soft Matter* **11**, 8058-8068 (2015).
18. J. Castillo-Tejas, S. Carro, O. Manero, Shear Banding in Telechelic Associative Polymers by Molecular Dynamics. *ACS Macro Letters* **6**, 190-193 (2017).
19. J. Sprakel, E. Spruijt, J. van der Gucht, J. T. Padding, W. J. Briels, Failure-mode transition in transient polymer networks with particle-based simulations. *Soft Matter* **5**, (2009).
20. M. A. Fardin, B. Lasne, O. Cardoso, G. Gregoire, M. Argentina, J. P. Decruppe, S. Lerouge, Taylor-like vortices in Shear-Banding Flow of Giant Micelles. *Phys. Rev. Lett.* **103**, 028302 (2009).
21. M. A. Fardin, D. Lopez, J. Croso, G. Grégoire, O. Cardoso, G. H. McKinley, S. Lerouge, Elastic Turbulence in Shear Banding Wormlike Micelles. *Phys. Rev. Lett.* **104**, (2010).
22. A. K. Omar, Z. G. Wang, Shear-Induced Heterogeneity in Associating Polymer Gels: Role of Network Structure and Dilatancy. *Phys. Rev. Lett.* **119**, 117801 (2017).
23. S. Suzuki, T. Uneyama, T. Inoue, H. Watanabe, Nonlinear Rheology of Telechelic Associative Polymer Networks: Shear Thickening and Thinning Behavior of Hydrophobically Modified Ethoxylated Urethane (HEUR) in Aqueous Solution. *Macromolecules* **45**, 888-898 (2012).
24. Y. Hu, S. Q. Wang, A. M. Jamieson, Rheological and Rheooptical Studies of Shear-Thickening Polyacrylamide Solutions. *Macromolecules* **28**, 1847-1853 (1995).
25. N. Sarkar, D. Kershner, Rigid rod water-soluble polymers. *Journal of Applied Polymer Science* **62**, 393-408 (1996).
26. T. Funaki, T. Kaneko, K. Yamaoka, Y. Ohsedo, J. P. Gong, Y. Osada, Y. Shibasaki, M. Ueda, Shear-Induced Mesophase Organization of Polyanionic Rigid Rods in Aqueous Solution. *Langmuir* **20**, 6518-6520 (2004).
27. Z. L. Wu, M. Arifuzzaman, T. Kurokawa, K. Le, J. Hu, T. L. Sun, H. Furukawa, H. Masunaga, J. P. Gong, Supramolecular Assemblies of a Semirigid Polyanion in Aqueous Solutions. *Macromolecules* **46**, 3581-3586 (2013).
28. Y. Wang, J. Gao, T. J. Dingemans, L. A. Madsen, Molecular Alignment and Ion Transport in Rigid Rod Polyelectrolyte Solutions. *Macromolecules* **47**, 2984-2992 (2014).

29. J. Gao, Y. Wang, B. Norder, S. J. Garcia, S. J. Picken, L. A. Madsen, T. J. Dingemans, Water and sodium transport and liquid crystalline alignment in a sulfonated aramid membrane. *J Memb Sci.* **489**, 194-203 (2015).
30. Y. Wang, Y. Chen, J. Gao, H. G. Yoon, L. Jin, M. Forsyth, T. J. Dingemans, L. A. Madsen, Highly Conductive and Thermally Stable Ion Gels with Tunable Anisotropy and Modulus. *Adv. Mater.* **28**, 2571-2578 (2016).
31. Y. Wang, Y. He, Z. Yu, J. Gao, S. Ten Brinck, C. Slebodnick, G. B. Fahs, C. J. Zanelotti, M. Hegde, R. B. Moore, B. Ensing, T. J. Dingemans, R. Qiao, L. A. Madsen, Double helical conformation and extreme rigidity in a rodlike polyelectrolyte. *Nat. Commun.* **10**, 801 (2019).
32. W. Yang, H. Furukawa, Y. Shigekura, K. Shikinaka, Y. Osada, J. P. Gong, Self-Assembling Structure in Solution of a Semirigid Polyelectrolyte. *Macromolecules* **41**, 1791-1799 (2008).
33. S. A. Safran, P. A. Pincus, M. E. Cates, F. C. MacKintosh, Growth of Charged Micelles. *J. Phys. France* **51**, 503-510 (1990).
34. F. C. Mackintosh, S. A. Safran, P. A. Pincus, Self-Assembly of Linear Aggregates: the Effect of Electrostatics on Growth. *Europhys. Lett.* **12**, 697-702 (1990).
35. M. E. Cates, Reptation of living polymers- dynamics of entangled polymers in the presence of reversible chain-scission reactions. *Macromolecules* **20**, 2289-2296 (1987).
36. S. Dou, R. H. Colby, Solution Rheology of a Strongly Charged Polyelectrolyte in Good Solvent. *Macromolecules* **41**, 6505-6510 (2008).
37. A. V. Dobrynin, R. H. Colby, M. Rubinstein, Scaling Theory of Polyelectrolyte Solutions. *Macromolecules* **28**, 1859-1871 (1995).
38. M. Rubinstein, R. H. Colby, A. V. Dobrynin, Dynamics of semidilute polyelectrolyte solutions. *Phys. Rev. Lett.* **73**, 2776-2779 (1994).
39. M. Doi, Molecular dynamics and rheological properties of concentrated solutions of rodlike polymers in isotropic and liquid crystalline phases. *Journal of Polymer Science: Polymer Physics Edition* **19**, 229-243 (1981).
40. R. F. Kayser, H. J. Raveché, Bifurcation in Onsager's model of the isotropic-nematic transition. *Physical Review A* **17**, 2067-2072 (1978).
41. G. J. Vroege, H. N. W. Lekkerkerker, Phase transitions in lyotropic colloidal and polymer liquid crystals. *Rep. Prog. Phys.* **55**, 1241-1309 (1992).
42. H. N. W. Lekkerkerker, P. Coulon, R. Van Der Haegen, R. Deblieck, On the isotropic-liquid crystal phase separation in a solution of rodlike particles of different lengths. *The Journal of Chemical Physics* **80**, 3427-3433 (1984).
43. G. J. Vroege, H. N. W. Lekkerkerker, Theory of the isotropic-nematic-nematic phase separation for a solution of bidisperse rodlike particles. *J. Phys. Chem.* **97**, 3601-1605 (1993).
44. L. Walker, N. Wagner, Rheology of region I flow in a lyotropic liquid-crystal polymer: The effects of defect texture. *Journal of Rheology* **38**, 1525-1547 (1994).
45. S. Onogi, T. Asada, *Rheology and Rheo-Optics of Polymer Liquid Crystals*. (1980).
46. M. E. Cates, S. M. Fielding, Rheology of giant micelles. *Advances in Physics* **55**, 799-879 (2006).
47. J. W. McAllister, J. R. Lott, P. W. Schmidt, R. L. Sammler, F. S. Bates, T. P. Lodge, Linear and Nonlinear Rheological Behavior of Fibrillar Methylcellulose Hydrogels. *ACS Macro Letters* **4**, 538-542 (2015).
48. F. C. MacKintosh, J. Kas, P. A. Janmey, Elasticity of semiflexible biopolymer networks. *Phys. Rev. Lett.* **75**, 4425-4428 (1995).
49. M. L. Gardel, J. H. Shin, F. C. MacKintosh, L. Mahadevan, P. Matsudaira, D. A. Weitz, Elastic Behavior of Cross-Linked and Bundled Actin Networks. *Science* **304**, 1301-1305 (2004).
50. W. W. Graessley, S. F. Edwards, Entanglement interactions in polymers and the chain contour concentration. *Polymer* **22**, 1329-1334 (1981).
51. N. Y. Yao, C. P. Broedersz, Y. C. Lin, K. E. Kasza, F. C. Mackintosh, D. A. Weitz, Elasticity in ionically cross-linked neurofilament networks. *Biophys J* **98**, 2147-2153 (2010).